

1 **Meis transcription factors regulate cardiac conduction system development and adult function**

2  
 3 Noelia Muñoz-Martín<sup>1</sup> PhD, Ana Simon-Chica<sup>2</sup> MSc, Covadonga Díaz-Díaz<sup>1</sup> PhD; Vanessa Cadenas<sup>1,3</sup>,  
 4 Susana Temiño<sup>1,3</sup>, Isaac Esteban<sup>1</sup> PhD, Andreas Ludwig<sup>4</sup> MD, PhD, Barbara Schormair<sup>5</sup> PhD, Juliane  
 5 Winkelmann<sup>5</sup> MD PhD, Veronika Olejnickova<sup>6</sup> PhD DVM, David Sedmera<sup>6</sup>, MD PhD, David Filgueiras-  
 6 Rama<sup>2,3,7</sup>, MD PhD, Miguel Torres<sup>1,3,\*</sup> PhD

7  
 8  
 9  
 10 1 Cardiovascular Regeneration Program, Centro Nacional de Investigaciones Cardiovasculares (CNIC),  
 11 Madrid, 28029, Spain

12 2 Novel Arrhythmogenic Mechanisms Program, Centro Nacional de Investigaciones Cardiovasculares  
 13 (CNIC), Madrid, 28029, Spain

14 3 Centro de Investigación Biomédica en Red de Enfermedades Cardiovasculares (CIBERCV). Madrid,  
 15 Spain

16 4 Institut für Experimentelle und Klinische Pharmakologie und Toxikologie, Friedrich-Alexander-  
 17 Universität Erlangen-Nürnberg, Germany

18 5 Institute of Neurogenomics, Helmholtz-Zentrum, Munich, Germany

19 6 Institute of Anatomy, First Faculty of Medicine, Charles University, Prague, Czech Republic

20 7 Instituto de Investigación Sanitaria del Hospital Clínico San Carlos (IdISSC), Madrid, Spain

21

22

23

24

25 \* Corresponding author

26 **Address:** Centro Nacional de Investigaciones Cardiovasculares. 3, Melchor Fernández Almagro. Madrid  
 27 28029. Spain

28 **Email:** [mtorres@cnic.es](mailto:mtorres@cnic.es) **Phone** +34 914531200. **Fax** +34 914531265

29

30 Short Title: Meis Factors in the Cardiac Conduction System

31

1 Category: Original Research

2

3 Total words: 10249

4

5

## 6 1. ABSTRACT

7

8 **AIMS:** The Cardiac Conduction System (CCS) is progressively specified during development by  
9 interactions among a discrete number of Transcriptions Factors that ensure its proper patterning and the  
10 emergence of its functional properties. Meis genes encode homeodomain transcription factors (TFs) with  
11 multiple roles in mammalian development. In humans, Meis genes associate with congenital cardiac  
12 malformations and alterations of cardiac electrical activity, however the basis for these alterations has not  
13 been established. Here we studied the role of Meis transcription factors in cardiomyocyte development and  
14 function during mouse development and adult life.

15

16 **METHODS AND RESULTS:** We studied *Meis1* and *Meis2* conditional deletion mouse models that  
17 allowed cardiomyocyte-specific elimination of Meis function during development and inducible  
18 elimination of Meis function in cardiomyocytes of the adult CCS. We studied cardiac anatomy, contractility  
19 and conduction. We report that Meis factors are global regulators of cardiac conduction, with a predominant  
20 role in the CCS. While constitutive Meis deletion in cardiomyocytes led to congenital malformations of the  
21 arterial pole and atria, as well as defects in ventricular conduction, Meis elimination in cardiomyocytes of  
22 the adult CCS produced sinus node dysfunction and delayed atrio-ventricular conduction. Molecular  
23 analyses unraveled Meis-controlled molecular pathways associated with these defects. Finally, we studied  
24 in transgenic mice the activity of a *Meis1* human enhancer related to an SNP associated by GWAS to PR  
25 elongation and found that the transgene drives expression in components of the atrio-ventricular conduction  
26 system.

27

28 **CONCLUSIONS:** Our study identifies Meis TFs as essential regulators of the establishment of cardiac  
29 conduction function during development and its maintenance during adult life. In addition, we generated  
30 animal models and identified molecular alterations that will ease the study of Meis-associated conduction  
31 defects and congenital malformations in humans.

32

33

34

35

## 2. INTRODUCTION

Meis transcription factors (TFs) belong to the TALE (Three Aminoacid Loop Extension) family and are highly conserved in evolution at the molecular and functional level<sup>1</sup>. *Meis1* (myeloid ecotropic viral integration site 1) was the first gene of the family to be identified<sup>2</sup>. In mammals, two additional highly similar genes have been identified; *Meis2* and *Meis3*<sup>3,4</sup>. Except in the head, the embryonic expression patterns of *Meis1* and *Meis2* are highly coincident and both genes encode very similar proteins with redundant functions<sup>5</sup>. In contrast, *Meis3* expression is mainly restricted to the hindbrain, although it can be also detected in the heart, spleen and lung at later stages<sup>4</sup>. Understanding Meis roles in cells in which *Meis1* and *Meis2* are co-expressed therefore involves the elimination of both genes.

*Meis* TFs function as cofactors of other TFs, such as Pbx, Prep or Hox factors<sup>6</sup>. They can form dimers or trimers, modifying the cofactors' affinity and selectivity for DNA-binding sites. Thus, there is increased difficulty in understanding *Meis* TFs function, because it is highly context-dependent. *Meis1* knockout mice die around E14.5 due to failing hematopoiesis<sup>7-9</sup>. Additional defects in *Meis1*-deficient embryos include eye hypoplasia, cardiac interventricular septum defects and overriding aorta<sup>7,9-11</sup>. *Meis2*-deficient mice also die around E14.5 and show hematopoietic defects and persistent truncus arteriosus<sup>12</sup>.

*Meis* TFs also play roles in postnatal life. *Meis1* is important for the maintenance of hematopoietic stem cell quiescence in the bone marrow hematopoietic niche<sup>13-15</sup>. In the postnatal heart, *Meis1* is important for the cell cycle arrest that takes place after birth in mouse cardiomyocytes<sup>16</sup>. In humans, a rare germline heterozygous *Meis2* mutation is associated with palatal defects, intellectual disability and congenital heart defects, including ventricular septal defect and overriding aorta<sup>17-19</sup>. In addition, *Meis1* genetic variants are associated with PR elongation in humans, suggesting a *Meis* role in atrio-ventricular conduction<sup>20,21</sup>. These results indicate that *Meis* TFs are not only involved in human heart morphogenesis, but also in the regulation of cardiomyocyte specialized functions, however this aspect has not been explored in animal models.

Genetic analyses in mouse models have advanced our knowledge on the transcriptional control of Cardiac Conduction System (CCS) development. Members of the Tbx-, GATA- and Irx-family, *Isl1*, *Nkx2.5*, *Shox2* and other TFs have been found essential for the specification and regional specialization of the CCS (reviewed in<sup>22</sup>). In contrast, the study of the role of developmental transcriptional regulatory networks during the maintenance of CCS physiology in the adult heart has remained less studied<sup>23,24</sup>.

Here, we studied the roles of *Meis1* and *Meis2* in cardiomyocytes using genetic mouse models. We report that *Meis* TFs are required for cardiac conduction with a predominant role in the cardiomyocytes of the CCS, including the sinoatrial node and the atrio-ventricular and ventricular conduction systems. Interestingly, *Meis* function is not restricted to CCS development but also required for the maintenance of

1 adult CCS physiology, including sinoatrial node pacemaker function and atrio-ventricular conduction. In  
2 particular, in the mouse models generated we observed elongation of the PR interval, which reproduces the  
3 GWAS association between *Meis1* and PR prolongation in humans. In addition, our study identifies  
4 congenital defects partially overlapping those reported in patients that carry *Meis2* mutations. Our study  
5 identifies Meis TFs as essential regulators of cardiac conduction development and adult physiology and  
6 provides animal models for *Meis*-associated conduction defects and congenital malformations.

### 10 3. METHODS

#### 12 **Mouse strains**

13 All animal procedures in the MT laboratory were approved by the CNIC Animal Experimentation Ethics  
14 Committee, by the Community of Madrid (Ref. PROEX 144.1/21) and conformed to EU Directive  
15 2010/63EU and Recommendation 2007/526/EC regarding the protection of animals used for experimental  
16 and other scientific purposes, enforced in Spanish law under Real Decreto 1201/2005. In this study mice  
17 were maintained on a mixed genetic background. Mice were euthanized by CO<sub>2</sub> inhalation according to the  
18 European Commission recommendations for the euthanasia of experimental animals.

19 Mouse lines used were *Meis1*<sup>ECFP</sup> and *Meis1*<sup>CreER</sup>11, *R26R*<sup>TdTomato</sup> 25, *Meis1*<sup>flox</sup> 13, *Meis2*<sup>flox</sup> 26, *α-MHC*<sup>Cre27</sup>,  
20 *Hcn4*<sup>CreERT2</sup> 28, and *617-HCRE* 29.

21 For the generation of M1M2KO mice, we crossed *Meis1*<sup>flox/flox</sup>; *Meis2*<sup>flox/flox</sup> females with *Meis1*<sup>flox+</sup>;  
22 *Meis2*<sup>flox/flox</sup>; *α-MHC*<sup>Cre/+</sup> males in order to obtain 25% of embryos with *Meis1* and *Meis2* double  
23 homozygous deletion. Animals resulting from the same crosses that did not inherit the Cre allele were used  
24 as controls.

25 For the generation of M1M2 CSiKO mice, we crossed *Meis1*<sup>flox/flox</sup>; *Meis2*<sup>flox/flox</sup> females with *Meis1*<sup>flox+</sup>;  
26 *Meis2*<sup>flox/flox</sup>; *Hcn4*<sup>CreERT2/+</sup> males in order to obtain 25% of embryos with *Meis1* and *Meis2* double  
27 homozygous deletion in the conduction system following Tamoxifen exposure. Animals resulting from the  
28 same crosses that did not inherit the CreERT2 allele were used as controls. For experiments, all animals  
29 received the same Tamoxifen dose, as described below.

#### 31 **Tamoxifen administration**

32 200 mg of tamoxifen (Sigma-T5648-1G) were dissolved in 20 ml of corn oil (Sigma-C8267) for a final  
33 concentration of 10 mg/ml. A daily dose of 100 μl from this solution was administered by oral-gavage to  
34 adult mice for 5 consecutive days.

## 1 **Immunofluorescence**

2 Hearts dissected and fixed overnight at 4°C in 2% paraformaldehyde (PFA) in PBS and whole/mount  
3 stained or embedded in gelatin or paraffin for sectioning. Primary antibodies used were anti-Meis1  
4 (1:500)<sup>30</sup>, anti-Meis2 (1:500)<sup>30</sup>, cTnT (1:200, MS-295 Thermo Scientific), Cx43 (1:200, Sigma C6219),  
5 GFP (1:200, Acris R1091P), Hcn4 (1:100, Abcam ab85023 and 1:200 Sigma-Aldrich AB5808), Cx40  
6 (1:200, Invitrogen 378900), Scn5a (1:200, Alomone Labs ASC-005). Cryosections or paraffin sections  
7 were permeabilized with PBT (PBS with 0.5% Triton X-100) and blocked with universal TNB blocking  
8 reagent FP1012-Perkin Elmer. Primary antibodies were incubated at 4°C overnight and secondary  
9 antibodies for 1 h at room temperature. Secondary antibodies were anti-rabbit Alexa633 and 594 (Life  
10 technologies A21071 and A11012), anti-rabbit-HRP (Dako P0448), anti-mouse Alexa488 (Life  
11 technologies A11029) and anti-goat-biotin (Jackson 705-065-003) all at 1:500 concentration. Sections were  
12 mounted using Dako fluorescence mounting medium (s3023). Whole-mount atria were stained with Wheat  
13 Germ Agglutinin (WGA-Thermo Scientific-W21404) and optically cleared using Abberior TDE Mounting  
14 Medium.

## 16 ***In situ* hybridization on sections**

17 Paraffin sections were rehydrated from xylol to PBS passing through sterile solutions with decreasing  
18 concentrations of ethanol. Sections were digested with proteinase K (10µg/ml) at 37°C for 10 minutes.  
19 Riboprobe hybridization was performed at 65°C overnight. The next day, sections were washed and  
20 incubated with anti-DIG antibody at 4°C overnight. Then, sections were developed with BM-purple (Roche,  
21 ref 11442074001) at room temperature or 37°C. Time of development was about 5 days.

## 23 **Image acquisition and analysis**

24 Images of the *in situ* hybridization were acquired with a Nikon Eclipse 90i microscope. H&E and Sirius  
25 Red stained sections were scanned with Hamamatsu Nanozoomer 2.0 RS and NDP. Scan 2.5 software.  
26 Analysis and quantifications were performed with the NDP Analyzer software.

27 Immunofluorescence images were acquired with a Zeiss LSM 700 confocal microscope using 405, 458,  
28 488, 568 and 633 nm wavelengths and 10x/0.45 dry, 25x/0.8 and 40x/1.3 oil objectives. Whole-mount atria  
29 3D images were obtained with the Leica TCS SP8 coupled to a DMi8 inverted confocal microscope  
30 Navigator module equipped with light laser. Z-stacks were captured every 4 µm using a 10x/0.4 dry  
31 objective. To estimate ploidy in isolated cardiomyocytes, nuclear volumes and DAPI intensity were  
32 measured with acquired confocal z-stacks at high magnification (63x/1.4, oil) with 2µm Z-steps using a  
33 Zeiss LSM 700 confocal microscope. Image J (<https://imagej.nih.gov/ij/>) was used for image analysis.

34

## 1 **Echocardiography**

2 For prenatal echocardiography, pregnant females were anesthetized with 2% isoflurane in oxygen.  
3 Abdominal surgery was then performed for uterus exposure. After surgery, isoflurane was adjusted to  
4 maintain a heart rate at  $450 \pm 50$  bpm and fetuses were exposed one at a time to keep them as warm as  
5 possible. An infrared heat lamp was used for the same purpose during acquisition. Echocardiography was  
6 performed by an expert operator using a high-frequency ultrasound system (Vevo 2100, Visualsonics,  
7 Canada) with a 50-MHz probe on a heating platform. Bidimensional (2D), M-Mode echocardiography was  
8 used to visualize the hearts in long and short axis view (LAX and SAX, respectively). Left and right  
9 ventricular ejection fraction (EF), wall thickness and diastolic and systolic chamber dimensions were  
10 assessed from the M-Mode SAX view. Ejection fraction was calculated from the short axis view at the level  
11 of the papillary muscles and using the Teichholz method<sup>31</sup>. Heart rate was calculated using three  
12 consecutive outflow waves. Corrected ventricular masses were calculated from M-mode images according  
13 to the following formula for the left ventricle:  $1.053 \times [(LVIDd + LVPWd + VSTd)^3 - (LVIDd)^3] \times 0.8$ ,  
14 where LVIDd: diastolic left ventricle inner dimension, LVPW: diastolic left ventricle posterior wall  
15 thickness and VSTd: ventricular septum thickness. The procedure for RV mass estimation was similar,  
16 taking into account that before birth both ventricles are rather similar and both serve the systemic  
17 circulation. The position of the fetuses was recorded, so that fetal identity could be tracked for genotyping.  
18 This procedure was therefore blinded to the genotype of the fetuses. A similar procedure was performed  
19 for adult mouse heart echography without surgery.

## 21 **Optical mapping**

22 Pregnant females at ED14.5 or ED16.5 were sacrificed by cervical dislocation and the embryos were  
23 harvested. Heart isolation from the embryos was performed in a petri dish with ice-cold Tyrode's Buffer to  
24 prevent ischemic damage. Harvested hearts were placed in wells of a P12 dish on ice and incubated for 15  
25 minutes in 500  $\mu$ L of ice-cold Tyrode's Buffer with 25  $\mu$ L of di-4-ANEPPS (stock solution in DMSO, 1.25  
26 mg/ml, Invitrogen) and 2  $\mu$ L of blebbistatin (14 mM stock in DMSO, Sigma) in darkness. After staining,  
27 hearts were pinned in a custom-made heated dish (37 °C) with continuously oxygenated Tyrode's Buffer  
28 with 14  $\mu$ M blebbistatin. Membrane voltage changes were recorded as fluorescence changes over time at 1  
29 kHz from both anterior and posterior aspect of the heart using Ultima L high-speed camera (SciMedia,  
30 Japan) and bundled software (BV\_Analyzer) was used to generate epicardial activation maps as described<sup>32</sup>.

## 32 **Electrocardiogram**

33 Electrocardiogram (ECG) recordings were obtained in sedated animals as reported elsewhere<sup>33</sup>. Briefly,  
34 mice were anesthetized with 1.5% isoflurane in oxygen, inhaled through a facial mask. To avoid night-day

1 circadian variations, ECGs were performed in the morning. Expert operators (V.C. and S.T.) gently handled  
2 the animals to insert subcutaneously ECG electrodes in the terminal end of the four limbs. Additional ECG  
3 gel was used to improve signal-to-noise ratio. Then, ECG recordings were acquired for 60-second at 2 KHz  
4 sweep-speed using a MP36R data acquisition workstation (Biopac Systems). Data were stored for off-line  
5 analysis using custom MatLab scripts for pre-processing, visualization and quantification of  
6 electrophysiological intervals and heart rate<sup>34</sup> (Figure S1).

7 After band-pass filtering between 0.5-200 Hz, baseline wander was removed using a bidirectional filtering  
8 strategy. We removed and excluded ECG segments with noise artifacts manually using sequential  
9 previsualization of 10-s segments. To detect the R-peak of the QRS complex (green dots in Figure S1), we  
10 used parabolic fitting of the Coiflet wavelet transformation and further detection of the maximum  
11 magnitude point. All R-peak detections were supervised to ensure accuracy of ECG segmentations. After  
12 detection of the QRS complex, P and T waves, and ECG intervals were extracted using adaptive windowing  
13 depending on beat-to-beat R-R changes. More specifically: i) PR intervals were measured from the  
14 beginning of the P wave to the beginning of the R wave/Q wave; ii) QRS intervals were measured from the  
15 beginning of the Q wave until the point where the S wave crosses the baseline; and iii) QT intervals were  
16 measured from the beginning of the Q wave until the point where the T-wave declines to 90% (T90) from  
17 the peak. Adaptive heart-rate-corrected QT values (QTc) were derived using a modification of Bazzer's  
18 formula for murine electrocardiography<sup>35</sup>. From the evaluation of control mice at 2 and 6 months of age,  
19 we established a sub-domain of normal RR variability among all ECG traces. Then, we defined the presence  
20 of sinus node dysfunction when the animal-specific  $RR_{n+1}$  vs  $RR_n$  domain fell partially or completely out  
21 of the normal RR variability sub-domain identified in controls. Dimensionless R-R intervals were also  
22 plotted over the 60-second electrogram recordings to detect sinus rhythm alterations. A free copy of the  
23 custom-made ECG tool for semiautomatic analysis of large amounts of data from long-duration ECG  
24 recordings in mice can be obtained from D.F. upon request.

## 25 26 **RNA sequencing**

27 4 control and 4 M1M2DKO fetuses were harvested at E15.5 from four independent litters. Hearts were  
28 dissected in ice-cold sterile PBS. Atria and ventricles were separated and OFT removed. Then, atria and  
29 ventricles were separated and all other tissues removed. Tissue lysis was performed with TissueLyser LT  
30 (Quiagen) or TriReagent (Trizol, Sigma-T9424) and RNA isolation with RNeasy Mini or Midi Kit  
31 (Quiagen) for embryonic and adult tissues respectively. Library and sequencing were performed at CNIC  
32 Genomic Unit. 20ng of total RNA were used to generate barcoded RNA-seq libraries using the NEBNext  
33 Ultra RNA Library preparation kit (New England Biolabs). The size and the concentration of the libraries  
34 was checked using the TapeStation 2200 DNA 1000 chip. Libraries were sequenced on a HiSeq2500

1 (Illumina) to generate 60-base single reads. FastQ files for each sample were obtained using bcltofastQ  
2 software 2.20. Gene Set Enrichment Analysis was performed with genes differentially expressed using the  
3 Broad Institute GSEA “Molecular Signatures Database” computing overlaps with KEGG and Gene  
4 Ontology gene sets. RNAseq data are available from the GEO database with accession number GSE213356.  
5

## 6 **Bioinformatic analysis**

7 Public Meis1 ChIP-seq data<sup>36</sup> was integrated with available ATAC-seq data from right atrial CMs  
8 and pacemaker CMs<sup>37</sup>. Raw ATAC-seq sequencing data was processed in order to obtain a list of  
9 accessible DNA regions. Adapters were trimmed using Cutadapt v.1.7.1<sup>38</sup> and reads were mapped  
10 against mouse mm10 reference genome using bowtie2 v.2.2.5<sup>39</sup>. Duplicated sequences were  
11 annotated with Markduplicates v.1.97 from the “Picard Tools”, Broad Institute GitHub repository  
12 (<http://broadinstitute.github.io/picard/>). Unmapped sequences, secondary alignments and low  
13 quality reads were filtered out. Peaks were called using MACS2 v.2.2.9.1<sup>40</sup> callpeaks function with  
14 the parameters --nomodel --shift -100 --extsize 200 commonly used for ATAC-seq data.  
15 Overlapping peaks between ChIP-seq and ATAC-seq data were obtained using the  
16 GenomicRanges<sup>41</sup> package in R. ATAC reads inside Meis1 peaks were quantified using the  
17 samtools v.0.1.18<sup>42</sup> bedcov function, and normalized by mapped library size.  
18

## 19 **Statistical analysis**

20 All statistical analyses are detailed in the figure legends.

## 21 **4. RESULTS**

### 22 **Meis1 and Meis2 expression in the developing and adult mouse heart**

23  
24 To characterize Meis function in cardiomyocytes, we studied the expression of *Meis1* and *Meis2* in the  
25 developing and adult mouse heart. In the embryonic heart, up to embryonic day of development 10.5  
26 (E10.5), *Meis1* and *Meis2* mRNA expression was detected in the second heart field, epicardium and  
27 endocardium, but not in the heart tube, indicating that Meis TFs associate at these early stages with a cardiac  
28 progenitor phenotype (Figure 1A). In contrast, from mid-gestation towards birth, Meis proteins revealed  
29 with a pan-Meis antibody were detected in differentiating cardiomyocytes (Figure 1B; 1C-E). Specific  
30 detection of *Meis1* expression using an ECFP knock-in reporter<sup>11</sup> showed at mid-gestation strong  
31 expression in the sino-atrial node, atrio-ventricular bundle, trabecular myocardium and atrial myocardium  
32 (Figure 1C'-E'). Lower expression levels were detected in the ventricular working myocardium (Figure  
33



1 1D'). Specific detection of *Meis2* showed generalized expression in cardiomyocytes, with higher  
2 expression in the atrio-ventricular bundle (AVB) (Figure 1F-H'). In the adult heart, both the *Meis1* reporter  
3 and the pan-*Meis* antibody showed a strong signal the sino-atrial node (SAN), atrio-ventricular node (AVN)  
4 and AVB (Figure 1I-K, M, N), a lower level of expression in atrial cardiomyocytes (Figure 1L-O) and very  
5 low expression in ventricular working cardiomyocytes (Figure 1P). Consistent with these results, tracing  
6 *Meis1*-expressing cells using knock-in *Meis1*<sup>CreERT2</sup> tracer line showed high density of labelled cells in the  
7 SAN, a medium density in atria and the bundle branches, and very low density in the working myocardium  
8 (Figure 1Q-S).

### 9 10 **Characterization of *Meis1* and *Meis2* function in cardiomyocytes**

11 To study the function of *Meis* TF in cardiomyocytes we recombined floxed *Meis1* and *Meis2* alleles with  
12  $\alpha$ MHC-Cre, generating double *Meis1* and *Meis2* disruption in cardiomyocytes (M1M2DKO) (Figure 2A,  
13 B). We did not recover any live M1M2DKO animal at postnatal day 1 (P1), while 60% were found alive  
14 at E18.5 (Figure 2C), indicating that most deaths took place at the end of gestation or perinatally.  
15 Anatomically, mutant hearts showed Ventricular Septum Defect (VSD), with inter-ventricular  
16 communication (60% of mutants) and overriding aorta (80% of hearts with VSD) (Figure 2D, G). In  
17 addition, atria were strongly dysmorphic, showing hypoplasia and finger like protrusions (Figure 2F).  
18 Evaluation of interventricular septum (IVS) thickness and ventricular mass by echocardiography at E18.5  
19 (Figure 2H) suggested mild hypoplasia of mutant hearts, while left ventricular function was preserved.  
20 Mutant hearts at E18.5 showed as well a higher beat rate than control hearts, suggesting alterations of the  
21 sino-atrial node.

22 We then studied by RNA-seq how the elimination of *Meis* function affects the cardiomyocyte molecular  
23 profile. For this, we separately analyzed the atria and ventricles of E15.5 M1M2DKO hearts. We found a  
24 high number of differentially expressed genes between mutants and controls in E15.5 atria and a lower  
25 number in ventricles at E15.5 (Figure 3A and Supplementary Datasets 1 and 2). This observation matches  
26 the expression profile of *Meis* genes and the strong dysmorphology of the atria in M1M2DKO hearts.

27 Pathway analysis of the differentially expressed genes (Figure 3B, C) identified an association with  
28 pathological conditions like Arrhythmogenic Right Ventricular Cardiomyopathy (ARVC), Hypertrophic  
29 Cardiomyopathy (HCM) and Dilated Cardiomyopathy (DCM). In relation to biological processes, "cardiac  
30 contraction" and "calcium signaling" were detected. The most prominent molecular pathways detected  
31 related to "GAP junction", "Focal adhesion", "ECM receptor interaction" and "Wnt signaling", suggesting  
32 the cell-cell and cell-ECM interactions were the most affected pathways.

1 To determine the validity of this analysis, we studied whether the differentially expressed genes were  
2 enriched for Meis1/2-bound genes, comparing our data with previously reported ChIP-seq data<sup>36</sup> that  
3 identified the distribution of Meis protein binding in the chromatin. We found a significant association  
4 between the genes differentially repressed or activated upon Meis inactivation and those genes that have  
5 nearby Meis1/2-binding sites in the heart<sup>36</sup> (Figure 3D and Supplementary Dataset 3). These results show  
6 that the RNA-seq analysis identifies direct Meis targets.

### 7 8 **Association of *Meis1* and *Meis2* function with CCS development and fetal function**

9 These previous observations, together with the preferential expression of *Meis1* and *Meis2* in various  
10 components of the adult CCS, led us to specifically address the role of Meis TFs in cardiac conduction. We  
11 therefore studied the correlation between Meis-regulated genes and a list of genes functionally associated  
12 with progressive CCS disease in humans<sup>43</sup> and found a strong association (Figure 4A). In addition, other  
13 studies identified Meis binding sites enriched in open chromatin regions in mouse sinoatrial node  
14 cardiomyocytes<sup>37</sup> and in human pacemaker-like cardiomyocytes derived from iPSCs<sup>44</sup>. We then mapped  
15 the co-occurrence of ATACseq peaks in RA and Pacemaker cardiomyocytes from<sup>37</sup> and Meis ChIPseq  
16 binding sites from<sup>36</sup> and associated them to specific genes by mapping their presence within -1Kb to +1Kb  
17 from the transcription units. We then identified the overlap between these genes and those that change  
18 expression in M1M2DKO mutants (Supplementary Dataset 4). This study showed that of the 1282 genes  
19 affected by Meis mutation in atria, 32% contained a Meis peak coincident with an ATACseq peak in RA  
20 CMs (Supplementary Dataset 4). This proportion was 35% for genes with Meis and ATACseq peaks in  
21 Pacemaker CMs. The identified genes represent good candidates for direct Meis targets in atrial and  
22 sinoatrial node CMs. There was a strong overlap between these candidate Meis targets in atrial and  
23 pacemaker CMs, with very few genes specific for atria, but a group of 50 genes specific for pacemaker  
24 CMs (Supplementary Dataset 4). Although the proportion of genes with ATACseq + Meis peaks was only  
25 slightly higher in Pacemaker CMs than in RA CMs, the opening of the ATACseq peaks coincident with  
26 Meis peaks was on average higher in Pacemaker CMs than in RA CMs, as measured by the number of reads  
27 in each peak (Figure 4B and Supplementary Dataset 5). The presence of ATACseq + Meis peaks was about  
28 double as frequent within the group of genes downregulated in mouse mutants than in the upregulated ones.  
29 This suggest that Meis is predominantly an activator rather than a repressor on direct targets in CMs. These  
30 results indicate Meis roles and target genes in both atrial and pacemaker CMs.

31 To more specifically study the correlation between genes regulated by Meis TF and the transcriptional  
32 signature of the CCS, we compared a published single-cell RNAseq analysis of the different components  
33 of the E16 CCS<sup>45</sup> with the set of genes de-regulated in E15.5 M1M2DKO hearts. We found a very strong

1 association between the genes downregulated in M1M2DKO (genes activated by Meis) and those found in  
2 the single-cell analysis to have preferential expression in the SAN, the AVN and the Purkinje (PKJ)  
3 cardiomyocytes (Figure 4C, left superior quadrant of each graph and Supplementary Datasets 6, 7 and 8).  
4 In contrast, genes downregulated in M1M2DKO are not found among those whose expression level in SAN,  
5 AVN or PKJ cardiomyocytes is similar or lower to that of surrounding non-CCS cardiomyocytes (Figure  
6 4C, left inferior quadrant of each graph + genes grouping around 0 in the vertical axis and Supplementary  
7 Datasets 6, 7 and 8). In contrast, genes upregulated in M1M2DKO (genes repressed by Meis) were found  
8 in both, the set of genes with higher expression in the SAN and AVN cardiomyocytes and the set of genes  
9 with lower expression in the SAN and AVN cardiomyocytes compared to surrounding non-CCS  
10 cardiomyocytes (Figure 4C, right upper and lower quadrants of each graph and Supplementary Datasets 6  
11 and 7). In the case of PKJ cardiomyocytes, genes upregulated in M1M2DKO only showed clear association  
12 with genes preferentially expressed in PKJ cardiomyocytes (Figure 4C, right upper quadrant and  
13 Supplementary Dataset 8). A study of the distribution of Meis ChIPseq peaks<sup>36</sup> showed that only genes with  
14 higher expression in SAN, AVN, or PKJ cardiomyocytes than in non-CCS cardiomyocytes strongly  
15 associate with Meis-bound genes (Figure 4D). To determine whether some of these findings correlate with  
16 expression changes at the level of protein expression, we characterized by immunocytochemistry the  
17 expression of SH2D4a, an adapter protein that regulates several signaling pathways<sup>46-48</sup>, is preferentially  
18 expressed in the SAN (Figure 4C and<sup>45</sup>) and shows lower expression in M1M2DKO atria by RNAseq  
19 (Figure 4C). We found widespread low expression of SH2D4a in cardiomyocytes of control mice, with the  
20 exception of the SAN, in which a strong expression was found (Figure S1). In M1M2DKO mutants,  
21 SH2D4a expression was strongly reduced in general and specifically in the SAN, where the strong  
22 expression was lost (Figure S1). We also tested the expression of the EPHB3 protein, a receptor involved  
23 in cell-cell communication that is preferentially expressed in the VCS (Figure 4C and<sup>45, 49</sup>) and shows  
24 reduced expression in M1M2DKO mutants by RNAseq (Figure 4C). In control hearts, we found expression  
25 of EPHB3 in the AVB, BB and subendothelial cardiomyocytes (Figure S1), the latter being coincident with  
26 the location of the Purkinje fibers. In M1M2DKO mutants we could not detect any EPHB3 expression  
27 (Figure S1). Together, these findings show that Meis controls the gene regulatory network typical of  
28 cardiomyocytes in various components of the CCS, with predominance of activating interactions, but also  
29 performing some repressive activities.

30 Next, we studied whether these changes in gene expression translate into functional alterations of cardiac  
31 conduction. For this, we first studied fetal cardiac conduction at E14.5 using an optical mapping approach  
32 to record epicardial voltage activation maps (Figure 4E). We found prolonged activation time in both, the  
33 right and the left ventricle (Figure 4E, F). No alterations were found in atrial conduction velocity in these  
34 analyses (not shown). The functional maturation of the His-Purkinje system can be monitored during

1 development by the progressive displacement of the breakthrough activation point from the base to the apex  
2 of the ventricles<sup>50,51</sup>. We therefore mapped the breakthrough point and found that in the LV it was more  
3 basally located in mutants compared to controls, while in the RV a non-significant but similar tendency  
4 was observed (Figure 4G). These observations indicate delayed maturation of the VCS, in agreement with  
5 the alterations found in gene expression.

### 7 ***Meis1* and *Meis2* maintain CCS function during adult life**

8 The previous results suggest a predominant role of Meis transcription factors in the development and adult  
9 physiology of components of the CCS; however, the M1M2DKO model does not sort out functions in  
10 working versus CCS cardiomyocytes and does not allow functional analyses in the adult heart. To  
11 overcome this limitation, we generated a model in which we used *Hcn4*<sup>CreERT2/28</sup> to specifically recombine  
12 the floxed Meis alleles in the CCS of adult mice (M1M2 CSiKO, Figure 5A-C). We administered  
13 Tamoxifen at 2 months of age and then followed the time-course of several ECG parameters (Figure 5D-  
14 K, S1) up to 24 months. As expected, the Tamoxifen treatment led to elimination of Meis expression in  
15 components of the CCS without obvious anatomical alterations (Figure S4). The analysis of the ECG  
16 showed an early (starting 1 month after tamoxifen administration) and statistically significant prolongation  
17 of the PR interval in mutants (Figure 5D). Time-course comparisons using a mixed model ANOVA also  
18 showed higher amplitude values of the P-wave in the M1M2 CSiKO mice compared to controls (Figure  
19 5E), without significant changes in P-wave duration between groups (Figure 5F). The prolongation of the  
20 PR interval suggests an underlying impairment of atrio-ventricular conduction in M1M2 CSiKO. In  
21 contrast, all analyses involving the QRS complex (QRS duration and amplitude) were not statistically  
22 different between mutants and controls (Figure 5G, H). The latter suggests no impairment in the VCS.  
23 Overall, heart rate values assessed using RR intervals were not statistically different between groups (Figure  
24 5I). However, further analysis using RR interval variability to address SAN function (in the absence of  
25 atrial or ventricular premature complexes) identified overt differences in RR interval variability between  
26 groups (Figure 5J, K). The latter was compatible with higher prevalence of sinus node dysfunction in  
27 mutants compared to controls. Such rhythm alterations were characterized by rapid oscillations in R-R  
28 intervals due to irregular P waves (with sinus node morphology) in singular or periodic episodes (Figure  
29 5L and S3). Moreover, further analysis of the time-course incidence of such alterations in RR interval  
30 variability showed early onset in M1M2CSiKO mice (already detected at 2 and 6 months after tamoxifen  
31 treatment in 5 out of 17 animals) compared to controls, in which only one animal showed abnormal RR  
32 interval variability at 24 months of age (Figure 5M and S3). In all animals, once sinus node dysfunction was  
33 detected, the alteration was present during the follow-up if the animal was still alive.

1 The elongation of the PR interval in M1M2 CSiKO mice evokes the human GWAS analyses in which  
2 *Meis1* SNPs located in intron 8 associate with PR interval elongation<sup>20,21</sup> (Figure 6A). Interestingly, SNP  
3 variants in intron 8 associate as well with the Restless Legs Syndrome (RLS) in humans<sup>52</sup> (Figure 6A), and  
4 a highly conserved regulatory element (*617-HCRE*) of the human *Meis1* intron 8 shows enhancer activity  
5 related to RLS<sup>29</sup> (Figure 6A). This regulatory element is nearby the lead SNP associated with PR interval  
6 elongation (rs10865355); however no functional SNP has been related yet to PR elongation in this region.  
7 Examination of previously described functional genomics data sets<sup>44,53</sup> shows that the only genomic  
8 segment with cardiac enhancer marks in the genomic region that contains SNPs in high linkage  
9 disequilibrium with rs10865355 is coincident with *617-HCRE* (Figure 6A). We thus studied the cardiac  
10 expression of a mouse transgene with the *LacZ* reporter under the control of the *617-HCRE* enhancer  
11 (Figure 6B). We found cardiac expression of the reporter in 6 out of 9 specimens. Expression was detected  
12 in small cell patches, which suggests variable mosaic expression of the transgene. In all 6 specimens, we  
13 found patches of cells potentially affecting the atrial and atrio-ventricular conduction system, including the  
14 SAN (Figure 6B, specimens #1, #2 and #5), the internodal tracks (Figure 6B, specimen #3) and the AVN  
15 (Figure 6B, specimen #4). Co-detection of  $\beta$ -Galactosidase with *Hcn4* in sections confirmed the expression  
16 of the transgene in cardiomyocytes of the SAN, AVN, AVB and adjacent regions (Figure 6C-E'). These  
17 results demonstrate that the *617-HCRE* activity contributes to *Meis1* expression in various components of  
18 the CCS, providing a potential mechanistic basis for the observed *Meis1*-linked PR elongation in humans.

19

## 20 5. DISCUSSION

21 Although *Meis2* is involved in human congenital malformations<sup>17-19</sup> and *Meis1* has been associated to PR  
22 elongation in humans<sup>20,21</sup> and to regenerative ability in mice<sup>16</sup>, a systematic analysis of *Meis1* and *Meis2*  
23 functions during the cardiomyocyte life cycle had not been performed. Given the strong similarity between  
24 *Meis1* and *Meis2* proteins and their frequent co-expression, we decided to perform a combined deletion of  
25 both genes in cardiomyocytes. A third gene encoding a transcription factor of the family, *Meis3*, is  
26 expressed at low levels in cardiomyocytes<sup>54</sup> and does not get activated in *Meis1/2* mutants (see RNAseq  
27 results). Therefore, the models reported here largely eliminate *Meis* function in cardiomyocytes. A detailed  
28 expression analysis revealed the preferential expression of *Meis1* and *Meis2* in the SAN, AVN and AVB  
29 cardiomyocytes and deletion of *Meis* genes showed alterations in cardiac conduction, both during  
30 development and in adult life. Interestingly, the observations in adult mice correlate well with the  
31 association of *Meis1* with PR elongation by GWAS in humans. Furthermore, we found that a mechanistic  
32 basis can be proposed between the activity of human *Meis1* enhancer *617-HCRE* and *Meis* function in  
33 cardiac conduction. In addition, we found alterations on sinus node function and impulse propagation in

1 the deletion of *Meis1* and *Meis2* from the adult CCS. These results suggest a wide involvement of Meis  
2 activity in regulating different components of the CCS, not only during development but, more intriguingly,  
3 during the maintenance of SAN pacemaker activity and atrio-ventricular conduction in adulthood. These  
4 observations suggest that not only congenital Meis mutations but alterations of Meis expression during  
5 adult life in cardiomyocytes of the SAN and atrio-ventricular conduction system may lead to progressive  
6 CCS disease. Interestingly, previous studies during limb induction have shown functional cooperation  
7 between Meis factors and Tbx5 through binding to common DNA sites<sup>55</sup>, while Tbx5 is required for VCS  
8 development and adult function maintenance<sup>56</sup>. Similarly, *Shox2*, which is needed for SAN development is  
9 also important for limb proximal-to-distal patterning and Meis TFs are upstream regulators of *Shox2*  
10 transcription during limb development<sup>55</sup>. In addition, *Nkx2.5* needs to be repressed from the prospective  
11 sinus node head for its proper specification<sup>57</sup> and *Meis1* has been shown to antagonize *Nkx2.5* on DNA  
12 binding sites during anterior SHF differentiation<sup>58</sup>. These correlations suggest that transcriptional  
13 regulatory modules involving Meis and other transcription factors co-opted during patterning of different  
14 organs.

15 In addition, VSD and atrial malformations were observed following Meis genes deletion during gestation,  
16 indicating functions beyond the development and function of the CCS. Although these morphological  
17 alterations could be envisioned as the cause of perinatal death of the mutants, functional analyses of fetuses  
18 at term do not detect heart failure, which suggests that perinatal electrical failure may underlie the observed  
19 lethality. The morphological alterations in atria are striking and suggest strong alteration of atrial patterning  
20 mechanisms. One of the pathways strongly altered in fetal hearts was the Wnt pathway and the factors  
21 involved preferentially contained those related to the planar cell polarity (PCP) pathway<sup>59</sup>, including ligands  
22 *Wnt5a* and *Wnt11* and receptors *Fzd1*, 4 and 7. Since the PCP pathway is generally involved in  
23 morphogenesis, it is likely involved in the morphological alterations found in the atria. Furthermore,  
24 deletion of *Wnt5a*<sup>60</sup>, *Wnt11*<sup>61</sup> and *Fzd1*<sup>62</sup> and *Fzd7*<sup>63</sup> leads to outflow tract defects including VSD, DORV,  
25 persistent truncus arteriosus and transposition of the great arteries, which suggests that the alterations of  
26 outflow tract patterning in Meis mutants are also related to failure in proper regulation of the PCP pathway.

27 Our study identifies multiple roles of Meis transcription factors during cardiomyocyte development and  
28 adult life and shows that they play a predominant role in the development and adult physiology of the SAN  
29 and atrio-ventricular conduction, providing models to explain the association between *Meis1* and cardiac  
30 conduction alterations in humans.

31

32

## 6. FUNDING

This work was supported by the European Commission H2020 Program [Grant number SC1 -BHC-07-2019. Ref. 874764 “REANIMA” to M.T.]; the Spanish Ministerio de Ciencia e Innovación [Grant numbers PGC2018-096486-B-I00 and PID2022-140058NB-C31 to M.T. and PID2019-109329RB-I00 to D.F.]; the Comunidad de Madrid [P2022/BMD-7245 CARDIOBOOST-CM to M.T.]; the Ministry of Education, Youth and Sports of the Czech Republic [Grant number Cooperation 207029 Cardiovascular Science to D.S.]; the Czech Science Foundation [Grant numbers 18-03461S and 22-05271S to D.S.]; ‘la Caixa’ Foundation Severo Ochoa PhD Fellowship [grant numbers 100010434 to N.M. and LCF/BQ/DR19/11740029 to A.S.]; EMBO short-term fellowship [Grant number 7667 to N.M.]; The CNIC is supported by the Ministerio de Ciencia e Innovación and the Pro CNIC Foundation, and is a Severo Ochoa Center of Excellence [Grant number CEX2020-001041-S].

## 7. AUTHOR CONTRIBUTIONS

**N.M.** Conceptualization, Experimentation, Methodology, Data Analysis, Manuscript Writing, Manuscript Correction

**A.S.** Data Analysis, Manuscript Correction

**C.D.** Immunofluorescence analyses

**S.T.** Methodology

**V.C.** Methodology

**I.E.** Methodology

**A.L.** Provision of transgenic mouse line

**B.S.** GWAS and LD data curation

**J.W.** Provision of transgenic mouse line, GWAS and LD data curation, and Manuscript Correction

**V.O.** Experimentation, Methodology

**D.S.** Conceptualization, Experimentation, Methodology, Data Analysis, Manuscript Correction

**D.F.** Conceptualization, Data Analysis, Manuscript Correction

1 M.T. Conceptualization, Experimentation, Methodology, Data Analysis, Manuscript Writing, Manuscript  
2 Correction

3

#### 4 8. ACKNOWLEDGEMENTS

5 We thank members of the Torres laboratory for fruitful discussions and advice on this work, Fátima  
6 Sánchez-Cabo for helpful advice on the statistics and Morena Raiola for help in Figure design. We thank  
7 the CNIC Technical Units for Compared Medicine, Advanced Imaging, Bioinformatics and Genomics.

8

9 Conflict of interest: none declared.

10

#### 11 9. REFERENCES

- 12 1. Longobardi E, Penkov D, Mateos D, De Florian G, Torres M, Blasi F. Biochemistry of the tale  
13 transcription factors PREP, MEIS, and PBX in vertebrates. *Developmental Dynamics*  
14 2014;**243**:59-75.
- 15 2. Moscow JA, Huang H, Carter C, Hines K, Zujewski J, Cusack G, Chow C, Venzon D, Sorrentino  
16 B, Chiang Y, Goldspiel B, Leitman S, Read EJ, Abati A, Gottesman MM, Pastan I, Sellers S,  
17 Dunbar C, Cowan KH. Engraftment of MDR1 and NeoR gene-transduced hematopoietic cells  
18 after breast cancer chemotherapy. *Blood* 1999;**94**:52-61.
- 19 3. Oulad-Abdelghani M, Chazaud C, Bouillet P, Sapin V, Chambon P, Dollé P. Meis2, a novel  
20 mouse Pbx-related homeobox gene induced by retinoic acid during differentiation of P19  
21 embryonal carcinoma cells. *Dev Dyn* 1997;**210**:173-183.
- 22 4. Nakamura T, Jenkins NA, Copeland NG. Identification of a new family of Pbx-related homeobox  
23 genes. *Oncogene* 1996;**13**:2235-2242.
- 24 5. Delgado I, Giovinazzo G, Temino S, Gauthier Y, Balsalobre A, Drouin J, Torres M. Control of  
25 mouse limb initiation and antero-posterior patterning by Meis transcription factors. *Nature*  
26 *communications* 2021;**12**:3086.
- 27 6. Mann RS, Affolter M. Hox proteins meet more partners. *Current opinion in genetics &*  
28 *development* 1998;**8**:423-429.
- 29 7. Azcoitia V, Aracil M, Martinez-A C, Torres M. The homeodomain protein Meis1 is essential for  
30 definitive hematopoiesis and vascular patterning in the mouse embryo. *Developmental biology*  
31 2005;**280**:307-320.
- 32 8. Carramolino L, Fuentes J, Garcia-Andres C, Azcoitia V, Riethmacher D, Torres M. Platelets play  
33 an essential role in separating the blood and lymphatic vasculatures during embryonic  
34 angiogenesis. *Circ Res* 2010;**106**:1197-1201.
- 35 9. Hisa T, Spence SE, Rachel RA, Fujita M, Nakamura T, Ward JM, Devor-Henneman DE, Saiki Y,  
36 Kutsuna H, Tessarollo L, Jenkins NA, Copeland NG. Hematopoietic, angiogenic and eye defects  
37 in Meis1 mutant animals. *The EMBO journal* 2004;**23**:450-459.
- 38 10. Stankunas K, Shang C, Twu KY, Kao SC, Jenkins NA, Copeland NG, Sanyal M, Selleri L,  
39 Cleary ML, Chang CP. Pbx/Meis deficiencies demonstrate multigenetic origins of congenital  
40 heart disease. *Circ Res* 2008;**103**:702-709.



- 1 11. Gonzalez-Lazaro M, Rosello-Diez A, Delgado I, Carramolino L, Angeles Sanguino M,  
2 Giovanazzo G, Torres M. Two New Targeted Alleles for the Comprehensive Analysis of Meis1  
3 Functions in the Mouse. *Genesis* 2014;**52**:967-975.
- 4 12. Machon O, Masek J, Machonova O, Krauss S, Kozmik Z. Meis2 is essential for cranial and  
5 cardiac neural crest development. *BMC Dev Biol* 2015;**15**:40.
- 6 13. Unnisa Z, Clark JP, Roychoudhury J, Thomas E, Tessarollo L, Copeland NG, Jenkins NA,  
7 Grimes HL, Kumar AR. Meis1 preserves hematopoietic stem cells in mice by limiting oxidative  
8 stress. *Blood* 2012;**120**:4973-4981.
- 9 14. Simsek T, Kocabas F, Zheng J, Deberardinis RJ, Mahmoud AI, Olson EN, Schneider JW, Zhang  
10 CC, Sadek HA. The distinct metabolic profile of hematopoietic stem cells reflects their location  
11 in a hypoxic niche. *Cell stem cell* 2010;**7**:380-390.
- 12 15. Kocabas F, Zheng J, Thet S, Copeland NG, Jenkins NA, DeBerardinis RJ, Zhang C, Sadek HA.  
13 Meis1 regulates the metabolic phenotype and oxidant defense of hematopoietic stem cells. *Blood*  
14 2012;**120**:4963-4972.
- 15 16. Mahmoud AI, Kocabas F, Muralidhar SA, Kimura W, Koura AS, Thet S, Porrello ER, Sadek HA.  
16 Meis1 regulates postnatal cardiomyocyte cell cycle arrest. *Nature* 2013;**497**:249-253.
- 17 17. Louw JJ, Corveleyn A, Jia Y, Hens G, Gewillig M, Devriendt K. MEIS2 involvement in cardiac  
18 development, cleft palate, and intellectual disability. *American journal of medical genetics Part A*  
19 2015;**167A**:1142-1146.
- 20 18. Verheije R, Kupchik GS, Isidor B, Kroes HY, Lynch SA, Hawkes L, Hempel M, Gelb BD,  
21 Ghomid J, D'Amours G, Chandler K, Dubourg C, Loddo S, Tumer Z, Shaw-Smith C, Nizon M,  
22 Shevell M, Van Hoof E, Anyane-Yeboa K, Cerbone G, Clayton-Smith J, Cogne B, Corre P,  
23 Corveleyn A, De Borre M, Hjortshoj TD, Fradin M, Gewillig M, Goldmuntz E, Hens G, Lemyre  
24 E, Journal H, Kini U, Kortum F, Le Caignec C, Novelli A, Odent S, Petit F, Revah-Politi A,  
25 Stong N, Strom TM, van Binsbergen E, study DDD, Devriendt K, Breckpot J. Heterozygous loss-  
26 of-function variants of MEIS2 cause a triad of palatal defects, congenital heart defects, and  
27 intellectual disability. *European Journal Of Human Genetics* 2019;**27**:278-290.
- 28 19. Giliberti A, Curro A, Papa FT, Frullanti E, Ariani F, Coriolani G, Grosso S, Renieri A, Mari F.  
29 MEIS2 gene is responsible for intellectual disability, cardiac defects and a distinct facial  
30 phenotype. *European journal of medical genetics* 2020;**63**:103627.
- 31 20. Pfeufer A, van Noord C, Marcianti KD, Arking DE, Larson MG, Smith AV, Tarasov KV, Muller  
32 M, Sotoodehnia N, Sinner MF, Verwoert GC, Li M, Kao WH, Kottgen A, Coresh J, Bis JC, Psaty  
33 BM, Rice K, Rotter JI, Rivadeneira F, Hofman A, Kors JA, Stricker BH, Uitterlinden AG, van  
34 Duijn CM, Beckmann BM, Sauter W, Gieger C, Lubitz SA, Newton-Cheh C, Wang TJ, Magnani  
35 JW, Schnabel RB, Chung MK, Barnard J, Smith JD, Van Wagoner DR, Vasani RS, Aspelund T,  
36 Eiriksdottir G, Harris TB, Launer LJ, Najjar SS, Lakatta E, Schlessinger D, Uda M, Abecasis GR,  
37 Muller-Myhsok B, Ehret GB, Boerwinkle E, Chakravarti A, Soliman EZ, Lunetta KL, Perz S,  
38 Wichmann HE, Meitinger T, Levy D, Gudnason V, Ellinor PT, Sanna S, Kaab S, Witteman JC,  
39 Alonso A, Benjamin EJ, Heckbert SR. Genome-wide association study of PR interval. *Nature*  
40 *genetics* 2010;**42**:153-159.
- 41 21. Smith JG, Magnani JW, Palmer C, Meng YA, Soliman EZ, Musani SK, Kerr KF, Schnabel RB,  
42 Lubitz SA, Sotoodehnia N, Redline S, Pfeufer A, Muller M, Evans DS, Nalls MA, Liu Y,  
43 Newman AB, Zonderman AB, Evans MK, Deo R, Ellinor PT, Paltoo DN, Newton-Cheh C,  
44 Benjamin EJ, Mehra R, Alonso A, Heckbert SR, Fox ER, Candidate-gene Association Resource  
45 C. Genome-wide association studies of the PR interval in African Americans. *PLoS genetics*  
46 2011;**7**:e1001304.
- 47 22. van Eif VWW, Devalla HD, Boink GJJ, Christoffels VM. Transcriptional regulation of the  
48 cardiac conduction system. *Nature reviews Cardiology* 2018;**15**:617-630.
- 49 23. Frank DU, Carter KL, Thomas KR, Burr RM, Bakker ML, Coetzee WA, Tristani-Firouzi M,  
50 Bamshad MJ, Christoffels VM, Moon AM. Lethal arrhythmias in Tbx3-deficient mice reveal

- 1 extreme dosage sensitivity of cardiac conduction system function and homeostasis. *Proceedings*  
2 *of the National Academy of Sciences of the United States of America* 2012;**109**:E154-163.
- 3 24. Takeda M, Briggs LE, Wakimoto H, Marks MH, Warren SA, Lu JT, Weinberg EO, Robertson  
4 KD, Chien KR, Kasahara H. Slow progressive conduction and contraction defects in loss of  
5 Nkx2-5 mice after cardiomyocyte terminal differentiation. *Lab Invest* 2009;**89**:983-993.
- 6 25. Madisen L, Zwingman TA, Sunkin SM, Oh SW, Zariwala HA, Gu H, Ng LL, Palmiter RD,  
7 Hawrylycz MJ, Jones AR, Lein ES, Zeng H. A robust and high-throughput Cre reporting and  
8 characterization system for the whole mouse brain. *Nat Neurosci* 2010;**13**:133-140.
- 9 26. Delgado I, López-Delgado AC, Roselló-Díez A, Giovinazzo G, Cadenas V, Fernández-de-  
10 Manuel L, Sánchez-Cabo F, Anderson MJ, Lewandoski M, Torres M. Proximo-distal positional  
11 information encoded by an Fgf-regulated gradient of homeodomain transcription factors in the  
12 vertebrate limb. *Sci Adv* 2020;**6**:eaaz0742.
- 13 27. Agah R, Frenkel PA, French BA, Michael LH, Overbeek PA, Schneider MD. Gene  
14 recombination in postmitotic cells. Targeted expression of Cre recombinase provokes cardiac-  
15 restricted, site-specific rearrangement in adult ventricular muscle in vivo. *The Journal of clinical*  
16 *investigation* 1997;**100**:169-179.
- 17 28. Hoel E, Stieber J, Herrmann S, Feil S, Tybl E, Hofmann F, Feil R, Ludwig A. Tamoxifen-  
18 inducible gene deletion in the cardiac conduction system. *J Mol Cell Cardiol* 2008;**45**:62-69.
- 19 29. Spieler D, Kaffe M, Knauf F, Bessa J, Tena JJ, Giesert F, Schormair B, Tilch E, Lee H, Horsch  
20 M, Czamara D, Karbalai N, von Toerne C, Waldenberger M, Gieger C, Lichtner P, Claussnitzer  
21 M, Naumann R, Muller-Myhsok B, Torres M, Garrett L, Rozman J, Klingenspor M, Gailus-  
22 Durner V, Fuchs H, Hrabe de Angelis M, Beckers J, Holter SM, Meitinger T, Hauck SM,  
23 Laumen H, Wurst W, Casares F, Gomez-Skarmeta JL, Winkelmann J. Restless legs syndrome-  
24 associated intronic common variant in Meis1 alters enhancer function in the developing  
25 telencephalon. *Genome research* 2014;**24**:592-603.
- 26 30. Mercader N, Tanaka EM, Torres M. Proximodistal identity during vertebrate limb regeneration is  
27 regulated by Meis homeodomain proteins. *Development (Cambridge, England)* 2005;**132**:4131-  
28 4142.
- 29 31. Teichholz LE, Kreulen T, Herman MV, Gorlin R. Problems in echocardiographic volume  
30 determinations: echocardiographic-angiographic correlations in the presence of absence of  
31 asynergy. *The American journal of cardiology* 1976;**37**:7-11.
- 32 32. Sankova B, Benes J, Jr., Krejci E, Dupays L, Theveniau-Ruissy M, Miquerol L, Sedmera D. The  
33 effect of connexin40 deficiency on ventricular conduction system function during development.  
34 *Cardiovasc Res* 2012;**95**:469-479.
- 35 33. Rivera-Torres J, Calvo CJ, Llach A, Guzman-Martinez G, Caballero R, Gonzalez-Gomez C,  
36 Jimenez-Borreguero LJ, Guadix JA, Osorio FG, Lopez-Otin C, Herraiz-Martinez A, Cabello N,  
37 Vallmitjana A, Benitez R, Gordon LB, Jalife J, Perez-Pomares JM, Tamargo J, Delpon E, Hove-  
38 Madsen L, Filgueiras-Rama D, Andres V. Cardiac electrical defects in progeroid mice and  
39 Hutchinson-Gilford progeria syndrome patients with nuclear lamina alterations. *Proceedings of*  
40 *the National Academy of Sciences of the United States of America* 2016;**113**:E7250-E7259.
- 41 34. Filgueiras-Rama D, Vasilijevic J, Jalife J, Noujaim SF, Alfonso JM, Nicolas-Avila JA, Gutierrez  
42 C, Zamarreno N, Hidalgo A, Bernabe A, Cop CP, Ponce-Balbuena D, Guerrero-Serna G, Calle D,  
43 Desco M, Ruiz-Cabello J, Nieto A, Falcon A. Human influenza A virus causes myocardial and  
44 cardiac-specific conduction system infections associated with early inflammation and premature  
45 death. *Cardiovasc Res* 2021;**117**:876-889.
- 46 35. Mitchell GF, Jeron A, Koren G. Measurement of heart rate and Q-T interval in the conscious  
47 mouse. *The American journal of physiology* 1998;**274**:H747-751.
- 48 36. Nguyen NUN, Canseco DC, Xiao F, Nakada Y, Li S, Lam NT, Muralidhar SA, Savla JJ, Hill JA,  
49 Le V, Zidan KA, El-Feky HW, Wang Z, Ahmed MS, Hubbi ME, Menendez-Montes I, Moon J,  
50 Ali SR, Le V, Villalobos E, Mohamed MS, Elhelaly WM, Thet S, Anene-Nzeli CG, Tan WLW,  
51 Foo RS, Meng X, Kanchwala M, Xing C, Roy J, Cyert MS, Rothermel BA, Sadek HA. A

- 1 calcineurin-Hoxb13 axis regulates growth mode of mammalian cardiomyocytes. *Nature*  
2 2020;**582**:271-276.
- 3 37. Galang G, Mandla R, Ruan H, Jung C, Sinha T, Stone NR, Wu RS, Mannion BJ, Allu PKR,  
4 Chang K, Rammohan A, Shi MB, Pennacchio LA, Black BL, Vedantham V. ATAC-Seq Reveals  
5 an Isl1 Enhancer That Regulates Sinoatrial Node Development and Function. *Circ Res*  
6 2020;**127**:1502-1518.
- 7 38. Martin M. Cutadapt removes adapter sequences from high-throughput sequencing reads.  
8 *EMBnetjournal, North America* 2011;**17**:10-12.
- 9 39. Langmead B, Salzberg SL. Fast gapped-read alignment with Bowtie 2. *Nat Methods* 2012;**9**:357-  
10 359.
- 11 40. Zhang Y, Liu T, Meyer CA, Eeckhoutte J, Johnson DS, Bernstein BE, Nusbaum C, Myers RM,  
12 Brown M, Li W, Liu XS. Model-based analysis of ChIP-Seq (MACS). *Genome biology*  
13 2008;**9**:R137.
- 14 41. Lawrence M, Huber W, Pages H, Aboyoun P, Carlson M, Gentleman R, Morgan MT, Carey VJ.  
15 Software for computing and annotating genomic ranges. *PLoS computational biology*  
16 2013;**9**:e1003118.
- 17 42. Li H, Handsaker B, Wysoker A, Fennell T, Ruan J, Homer N, Marth G, Abecasis G, Durbin R,  
18 Genome Project Data Processing S. The Sequence Alignment/Map format and SAMtools.  
19 *Bioinformatics (Oxford, England)* 2009;**25**:2078-2079.
- 20 43. Asatryan B, Medeiros-Domingo A. Molecular and genetic insights into progressive cardiac  
21 conduction disease. *EP Europace* 2019;**21**:1145-1158.
- 22 44. van Eif VWW, Protze SI, Bosada FM, Yuan X, Sinha T, van Duijvenboden K, Ernault AC,  
23 Mohan RA, Wakker V, de Gier-de Vries C, Hooijkaas IB, Wilson MD, Verkerk AO, Bakkers J,  
24 Boukens BJ, Black BL, Scott IC, Christoffels VM. Genome-Wide Analysis Identifies an Essential  
25 Human TBX3 Pacemaker Enhancer. *Circ Res* 2020;**127**:1522-1535.
- 26 45. Goodyer WR, Beyersdorf BM, Paik DT, Tian L, Li G, Buikema JW, Chirikian O, Choi S,  
27 Venkatraman S, Adams EL, Tessier-Lavigne M, Wu JC, Wu SM. Transcriptomic Profiling of the  
28 Developing Cardiac Conduction System at Single-Cell Resolution. *Circ Res* 2019;**125**:379-397.
- 29 46. Li T, Li W, Lu J, Liu H, Li Y, Zhao Y. SH2D4A regulates cell proliferation via the  
30 ERalpha/PLC-gamma/PKC pathway. *BMB reports* 2009;**42**:516-522.
- 31 47. Ploeger C, Huth T, Sugiyanto RN, Pusch S, Goepfert B, Singer S, Tabti R, Hausser I,  
32 Schirmacher P, Desaubry L, Roessler S. Prohibitin, STAT3 and SH2D4A physically and  
33 functionally interact in tumor cell mitochondria. *Cell death & disease* 2020;**11**:1023.
- 34 48. Yuki R, Ikeda Y, Yasutake R, Saito Y, Nakayama Y. SH2D4A promotes centrosome maturation  
35 to support spindle microtubule formation and mitotic progression. *Scientific reports*  
36 2023;**13**:2067.
- 37 49. van Eif VWW, Stefanovic S, Mohan RA, Christoffels VM. Gradual differentiation and  
38 confinement of the cardiac conduction system as indicated by marker gene expression. *Biochim*  
39 *Biophys Acta Mol Cell Res* 2020;**1867**:118509.
- 40 50. Rentschler S, Vaidya DM, Tamaddon H, Degenhardt K, Sassoon D, Morley GE, Jalife J, Fishman  
41 GI. Visualization and functional characterization of the developing murine cardiac conduction  
42 system. *Development (Cambridge, England)* 2001;**128**:1785-1792.
- 43 51. Gurjarpadhye A, Hewett KW, Justus C, Wen X, Stadt H, Kirby ML, Sedmera D, Gourdie RG.  
44 Cardiac neural crest ablation inhibits compaction and electrical function of conduction system  
45 bundles. *Am J Physiol Heart Circ Physiol* 2007;**292**:H1291-1300.
- 46 52. Winkelmann J, Schormair B, Lichtner P, Ripke S, Xiong L, Jalilzadeh S, Fulda S, Putz B,  
47 Eckstein G, Hauk S, Trenkwalder C, Zimprich A, Stiasny-Kolster K, Oertel W, Bachmann CG,  
48 Paulus W, Peglau I, Eisensehr I, Montplaisir J, Turecki G, Rouleau G, Gieger C, Illig T,  
49 Wichmann HE, Holsboer F, Muller-Myhsok B, Meitinger T. Genome-wide association study of  
50 restless legs syndrome identifies common variants in three genomic regions. *Nature genetics*  
51 2007;**39**:1000-1006.

- 1 53. VanOudenhove J, Yankee TN, Wilderman A, Cotney J. Epigenomic and Transcriptomic  
2 Dynamics During Human Heart Organogenesis. *Circ Res* 2020;**127**:e184-e209.
- 3 54. O'Meara CC, Wamstad JA, Gladstone RA, Fomovsky GM, Butty VL, Shrikumar A, Gannon JB,  
4 Boyer LA, Lee RT. Transcriptional reversion of cardiac myocyte fate during mammalian cardiac  
5 regeneration. *Circ Res* 2015;**116**:804-815.
- 6 55. Delgado I, Giovinazzo G, Temiño S, Gauthier Y, Balsalobre A, Drouin J, Torres M. Control of  
7 mouse limb initiation and antero-posterior patterning by Meis transcription factors. *Nature*  
8 *communications* 2021;**12**:3086.
- 9 56. Burnicka-Turek O, Broman MT, Steimle JD, Boukens BJ, Petrenko NB, Ikegami K, Nadadar  
10 RD, Qiao Y, Arnolds DE, Yang XH, Patel VV, Nobrega MA, Efimov IR, Moskowitz IP.  
11 Transcriptional Patterning of the Ventricular Cardiac Conduction System. *Circ Res*  
12 2020;**127**:e94-e106.
- 13 57. Li H, Li D, Wang Y, Huang Z, Xu J, Yang T, Wang L, Tang Q, Cai CL, Huang H, Zhang Y,  
14 Chen Y. Nkx2-5 defines a subpopulation of pacemaker cells and is essential for the physiological  
15 function of the sinoatrial node in mice. *Development (Cambridge, England)* 2019;**146**.
- 16 58. Dupays L, Shang C, Wilson R, Kotecha S, Wood S, Towers N, Mohun T. Sequential Binding of  
17 MEIS1 and NKX2-5 on the Popdc2 Gene: A Mechanism for Spatiotemporal Regulation of  
18 Enhancers during Cardiogenesis. *Cell reports* 2015;**13**:183-195.
- 19 59. Yang Y, Mlodzik M. Wnt-Frizzled/planar cell polarity signaling: cellular orientation by facing  
20 the wind (Wnt). *Annual review of cell and developmental biology* 2015;**31**:623-646.
- 21 60. Schleiffarth JR, Person AD, Martinsen BJ, Sukovich DJ, Neumann A, Baker CV, Lohr JL,  
22 Cornfield DN, Ekker SC, Petryk A. Wnt5a is required for cardiac outflow tract septation in mice.  
23 *Pediatr Res* 2007;**61**:386-391.
- 24 61. Zhou W, Lin L, Majumdar A, Li X, Zhang X, Liu W, Etheridge L, Shi Y, Martin J, Van de Ven  
25 W, Kaartinen V, Wynshaw-Boris A, McMahon AP, Rosenfeld MG, Evans SM. Modulation of  
26 morphogenesis by noncanonical Wnt signaling requires ATF/CREB family-mediated  
27 transcriptional activation of TGFbeta2. *Nature genetics* 2007;**39**:1225-1234.
- 28 62. Yu H, Smallwood PM, Wang Y, Vidaltamayo R, Reed R, Nathans J. Frizzled 1 and frizzled 2  
29 genes function in palate, ventricular septum and neural tube closure: general implications for  
30 tissue fusion processes. *Development (Cambridge, England)* 2010;**137**:3707-3717.
- 31 63. Yu H, Ye X, Guo N, Nathans J. Frizzled 2 and frizzled 7 function redundantly in convergent  
32 extension and closure of the ventricular septum and palate: evidence for a network of interacting  
33 genes. *Development (Cambridge, England)* 2012;**139**:4383-4394.

34

35 **10. FIGURE LEGENDS**

36

37 **Figure 1. Expression of Meis1 and Meis2 in the developing and adult heart.** (A) *Meis1* and *Meis2*  
38 mRNA in situ hybridization showing expression in the second heart field (SHF), pericardium, endocardium  
39 (Ec) and epicardium (Ep) at E10.5. Boxed regions indicate magnifications shown in the panels to the right  
40 side. (B) Confocal images of ventricles at the indicated embryonic days. Anti-Meis1 immunofluorescence  
41 shown in red and myocardium autofluorescence in green. Boxed areas are magnified in the panels below.  
42 (C-E') Confocal images from sections of E16.5 hearts with the *Meis1*<sup>ECFP</sup> line combined with anti-Meis1.  
43 (F-H') Confocal images from sections of E16.5 hearts showing anti-Meis2 and anti-cTNT  
44 immunofluorescence. Boxes in C and F indicate magnified regions in D-E' and G-H'. CM, ventricular

1 compact myocardium; TM, trabecular myocardium (TM); MS, membranous septum (MS); AVB, atrio-  
 2 ventricular bundle (AVB). (I-L) Confocal images showing the distribution of ECFP in the CCS and atrial  
 3 myocardium of *Meis1<sup>ECFP</sup>* adult hearts. (M-P) Anti-Meisa and anti-Hcn4 immunofluorescence in the SAN  
 4 (M) and AVN (N), right atrium (O) and ventricular CMs (P). Dotted lines indicate magnified areas and  
 5 arrowheads within show anti-Meisa-positive CMs. (Q-Q') Whole-mount brightfield and fluorescent  
 6 confocal images of *Meis1<sup>CreER</sup>;R26R<sup>TdTomato</sup>* adult hearts showing strong recombination in the SAN  
 7 following Tamoxifen administration. Tamoxifen was administered by oral gavage to 10 week old mice at  
 8 a dose of 1mg/day for 5 consecutive days. Hearts were harvested two days after tamoxifen  
 9 administration. (R-S) 200 $\mu$ m-thick sections of the same heart, stained with DAPI and acquired by confocal  
 10 microscopy (maximum projection). (R) shows expression in RA and SAN and (S) expression in the bundle  
 11 branches (BB). CM, ventricular compact myocardium; TM, trabecular myocardium; MS, membranous  
 12 septum; AVB, atrio-ventricular bundle; OFT, Outflow tract; V, Ventricle; M, Myocardium; RA, Right  
 13 Atrium; LA, Left Atrium; LV, Left Ventricle; RV, Right Ventricle; SAN, Sinoatrial node; RBB, right and  
 14 left bundle branch; LBB left bundle branch. Scale bars: 100 $\mu$ m, except in Q (1 mm) and R (300  $\mu$ m).

15  
 16 **Figure 2. Anatomical and functional consequences of the elimination of *Meis1* and *Meis2* function in**  
 17 **cardiomyocytes during embryonic development.** (A) Model for simultaneous constitutive deletion of  
 18 *Meis1* and *Meis2* in CMs. (B) Confocal images of control and M1M2DKO embryos showing the loss of  
 19 Meis expression in mutant cardiomyocytes by immunofluorescence with anti-Meisa and cTNT. Boxes  
 20 indicate the magnified regions shown in the panels on the right side. Arrowheads point to cardiomyocyte  
 21 nuclei with or without Meis expression. Scale bars, 100  $\mu$ m. (C) Expected and observed frequencies of  
 22 M1M2DKO fetuses at different embryonic days. E. 14.5 n=72; E16.5 n=66; E18.5, n=130; P1, n=27. One-  
 23 Tailed Fischer's test. (D) Four-chamber view of E16.5 control and mutant embryonic heart sections stained  
 24 with H&E. Arrowheads point to VSD and RA morphology. Scale bar 200 $\mu$ m. (E) Ventral view of  
 25 representative whole-mount E18.5 hearts from control and mutant littermates. Arrowhead points to finger-  
 26 like projections in the left atrium. Scale bar 500 $\mu$ m. Panels on the right side show magnification of left atria  
 27 for better appreciation of the altered morphology. Scale bar 200 $\mu$ m. (F) 3D reconstruction of whole-mount  
 28 confocal images from E18.5 control and mutant atria stained with WGA. Arrowheads indicate finger-like  
 29 projections in the mutant atrium. Panels on the right side show individual confocal sections the  
 30 reconstructed specimens. Scale bar: 400 $\mu$ m. (G) Classification of M1M2DKO fetuses at E16.5 according  
 31 to the presence of ventricular septal defects (VSD). n=12. (H) Results from transuterine echocardiography  
 32 of control and mutant fetuses at 18.5. n=15 control and 9 mutant specimens for all graphs except for bmp,  
 33 in which 26 control and 18 mutant specimens were used. IVS, Interventricular septum thickness; LV, RV

1 mass, left and right ventricular mass corrected; LVEF left ventricular ejection fraction. Unpaired two-tailed  
 2 Mann-Whitney Test. Lines show the mean and dots, individual measurements on different specimens.

3  
 4 **Figure 3. Transcriptomic analysis of mutant hearts with cardiomyocyte-specific *Meis1* and *Meis2***  
 5 **deletion.** (A) Volcano plots showing transcriptome changes in atria (blue, above) and ventricles (red,  
 6 below) of E15.5 M1M2DKO hearts. n=4 control and 4 mutant specimens. Some genes potentially relevant  
 7 in cardiac biology are highlighted. For the analysis in atria, genes of the Gene Ontology class “Wnt  
 8 signaling pathway” are shown in green. (B-C) Gene ontology plots summarizing results from gene set  
 9 enrichment analysis in E15.5 M1M2DKO ventricles (B) and atria (C). Genes and fold changes are  
 10 represented on the left side, and the associated disease categories on the right side. (D) Graph showing the  
 11 overrepresentation of genes bound by *Meis1/2* (ChIPseq peaks from 3kb upstream to 1kb downstream; data  
 12 from<sup>36</sup>) within the genes activated ( $\geq 1.5$  fold) or repressed ( $\leq -1.5$  fold) in the RNA-seq analysis in E15.5  
 13 atria and ventricles. Chi-square test with two-tailed P values.

14  
 15 **Figure 4. Elimination of *Meis* function affects the cardiac conduction system during heart**  
 16 **development.** (A) Graphic table shows the incidence of *Meis* regulation and binding to genes associated  
 17 to progressive cardiac conduction disease. Blue filling indicates repression in M1M2DKO and red filling  
 18 activation in M1M2DKO of the indicated gene in the colored heart region. The presence of a *Meis1/2*  
 19 ChIPseq peak<sup>36</sup> from 3kb upstream to 1kb downstream of the transcription unit is represented by a ChIPseq  
 20 “peak” icon. Chi-square test with Yate’s correction and two-tailed P-values. (B) Violin plot representing  
 21 the distribution of reads/peak in ATACseq peaks<sup>37</sup> coincident with *Meis* ChIPseq binding sites<sup>36</sup> in RA  
 22 CMs (RACMs) and pacemaker CMs (PCMs). The dotted lines show the median and quartiles. Wilcoxon  
 23 matched-pairs signedrank test. Two tailed p-value < 0.0001. (C) Plots correlating single-cell RNA-seq fold-  
 24 change between CCS cardiomyocytes and nearby non-CCS cardiomyocytes from<sup>45</sup>, with RNA-seq fold  
 25 change upon *Meis1/2* elimination in cardiomyocytes. n=4 control and 4 mutant specimens for RNAseq of  
 26 *Meis* mutants. Dots highlighted in red indicate genes that change significantly in the *Meis1/2* mutant hearts.  
 27 From left to right, graphs show the comparison of *Meis1/2* mutant atria with the SAN region, *Meis1/2*  
 28 mutant atria with the AVN region and *Meis1/2* mutant ventricles with the VCS region. (D) Volcano plots  
 29 showing the distribution of single-cell RNA-seq fold-change between CCS cardiomyocytes and nearby  
 30 non-CCS cardiomyocytes from<sup>45</sup> with highlight of the genes bound by *Meis1/2* in ChIPseq adult heart  
 31 experiments from<sup>36</sup>. Line graphs below indicate the local enrichment in *Meis*-bound genes according to the  
 32 fold enrichment in the single-cell RNA-seq analyses. Data are shown from left to right for the SAN, AVN  
 33 and VCS regions. Chi-square test with Yate’s correction and two-sided P-values. (E) Representative optical  
 34 maps of ventricular depolarization (dorsal side) in control and M1M2DKO hearts at E14.5. (\*) indicates

1 the area where the first signal appears. Color bar shows the temporal scale (each color = 1 ms). Scale bar,  
 2 200  $\mu$ m. (F) Left and right ventricular activation curves showing depolarized area percentage per  
 3 millisecond obtained from the maps (n=8/group). Graphs show the mean  $\pm$ SEM. Two-way ANOVA with  
 4 Sidak's correction for multiple measurements and two-sided p-value. (G) Map of the ventricular conduction  
 5 activation points (or breakthrough point), indicated with an asterisk for each control and mutant hearts,  
 6 including representation of the geometric center and a standard deviation ellipse (dorsal view). n=6 control  
 7 and 7 mutant specimens. Type II MANOVA Test with Pillai statistics was applied to the orthogonal  
 8 coordinates defining the position of each activation point.

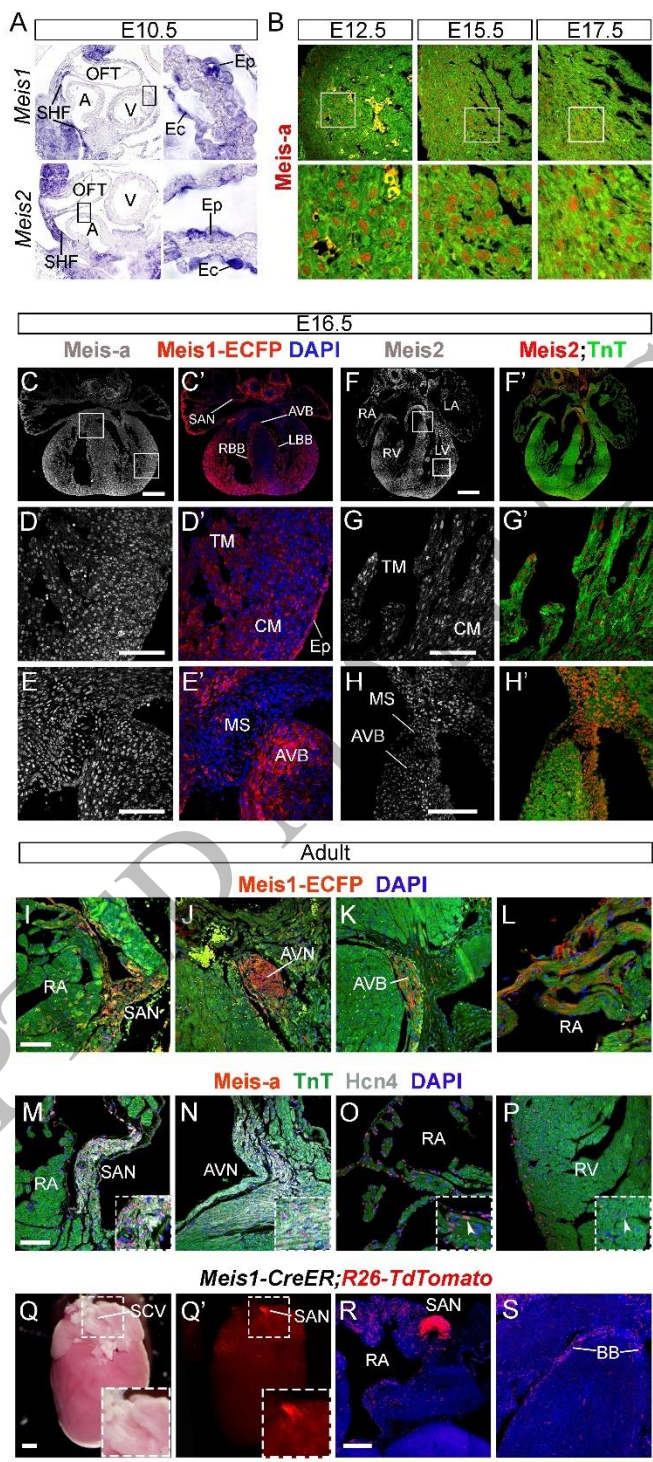
9  
 10 **Figure 5. Conditional elimination of Meis function in the adult cardiac conduction system produces**  
 11 **progressive dysfunction of sinus rhythm function and PR elongation.** (A) Model for double deletion of  
 12 *Meis1* and *Meis2* in the conduction system using *Hcn4<sup>CreERT2</sup>*. (B) Experimental timeline showing tamoxifen  
 13 treatment and the schedule for the electrocardiographic analyses. (C) Dorsal views in brightfield and  
 14 epifluorescence of a tamoxifen-induced newborn heart in which Tomato reports the sites of Cre activity  
 15 provided by the *Hcn4<sup>CreERT2</sup>* allele. SAN, sinoatrial node; AVN, atrioventricular node. Scale bar, 1 mm. (D-  
 16 I) Representation of the values for different parameters of the ECG analyses in control and mutant MIM2  
 17 CSiKO mice before tamoxifen administration (basal) and at different times after tamoxifen administration.  
 18 Each dot represents the average value for a single specimen. n=10 control and 16 mutant in Basal, 10 control  
 19 and 16 mutant at 1 and 2 months, 9 control and 17 mutant at 6 months and 3 control and 10 mutant at 24  
 20 months. Mixed model ANOVA with Sidak's correction for multiple measurements and two-tailed P values.  
 21 Adjusted P-values are shown for each individual comparison. The P-value for the global analysis of the  
 22 "genotype" variable is shown only in case of significance. (J) Examples of ECGs of control and MIM2  
 23 CSiKO showing sinus rhythm dysfunction. (K) Poincaré plot of the RR<sub>n</sub> to RR<sub>n+1</sub> correlation in relative  
 24 terms for all analyzed data in D-I (right). The domain for "no sinus node dysfunction" was determined from  
 25 control animals of up to 6 months of age, whereas all points outside this domain correspond to mutants up  
 26 to 6 months of age. (L) Example of sinus rhythm alteration in the same mutant specimen 6 months and 2  
 27 years after tamoxifen administration. (M) Bar plot showing the incidence of sinus node dysfunction in  
 28 control and mutant MIM2 CSiKO mice at different times after tamoxifen administration for all analyzed  
 29 data in D-I.

30  
 31 **Figure 6. A Meis1 human enhancer in a GWAS-identified intron associated with PR elongation drives**  
 32 **expression in CCS cardiomyocytes.** (A) The *Meis1* genomic region showing SNPs in different degrees of  
 33 linkage disequilibrium with the lead SNP associated with PR elongation (rs10865355). SNP linkage data  
 34 were retrieved from LD information from the European ancestry (EUR) dataset of the 1000Genomes Phase

1 3 project for rs10865355 using the LDproxy Tool provided by LDLink  
2 (<https://ldlink.nci.nih.gov/?tab=ldproxy>). The full list of SNPs is provided in Supplementary Dataset 9.  
3 Below, a zoom-in to intron 8, where the PR elongation-associated SNPs are located. Potential regulatory  
4 elements are indicated by epigenetic marks and detection of open chromatin by ATAC-seq in pace maker-  
5 like CMs and ventricular-like CMs derived from hiPSCs and the developing human heart. The location of  
6 the *617-HCRE* enhancer, previously characterized in the context of the RLS syndrome<sup>29</sup>, is also shown. (B)  
7 Scheme showing the transgene carrying *LacZ* gene under the control of *617-HCRE* and brightfield images  
8 of 5 different E17.5 transgenic hearts stained for LacZ. Arrowheads indicate the areas of LacZ expression.  
9 Ao, Aorta; Pa, pulmonary artery; SV, sinus venosus; AVVs, atrio-ventricular valves. Scale bars, 500  $\mu$ m.  
10 (C-E) Confocal images of co-immunofluorescence of  $\beta$ -Galactosidase (green) and Hcn4 (red) in sections  
11 from transgenic hearts at E17.5. Arrowheads indicate the areas of co-expression at the sino-atrial node  
12 (SAN), atrio-ventricular node (AVN) and atrio-ventricular bundle (AVB). (C'-E') Single channel images  
13 from panel C-E with  $\beta$ -Galactosidase expression.

14





1  
 2  
 3

Figure 1  
 144x264 mm (DPI)

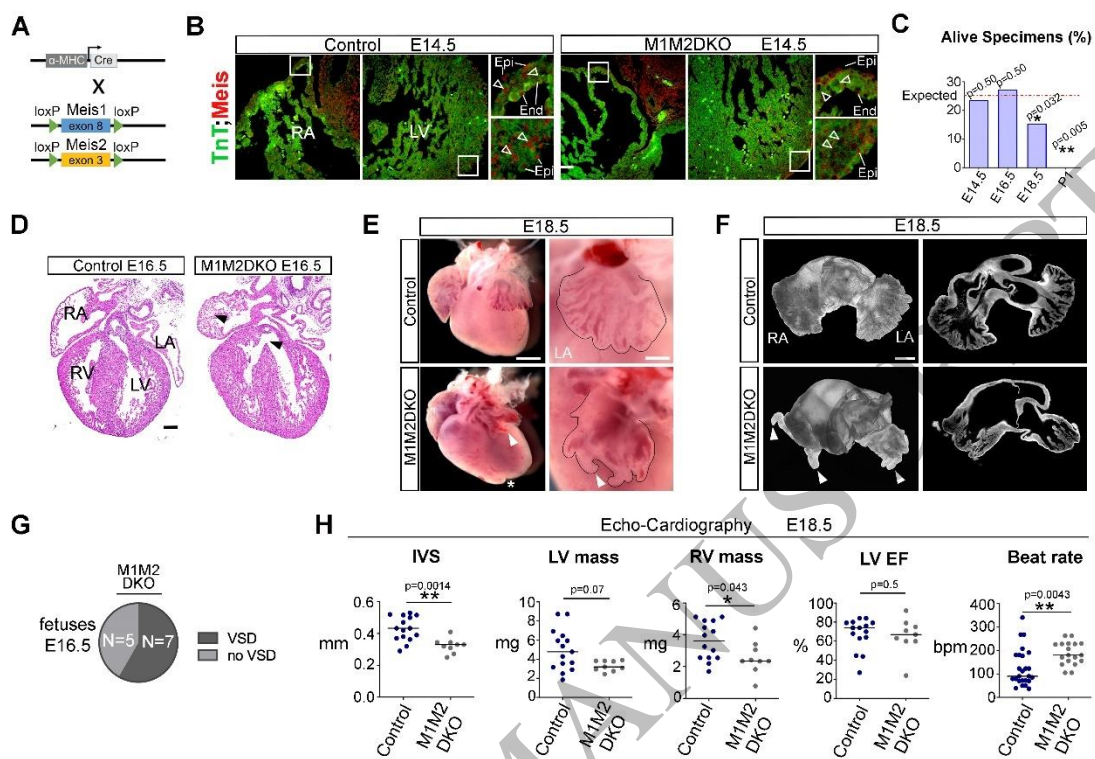
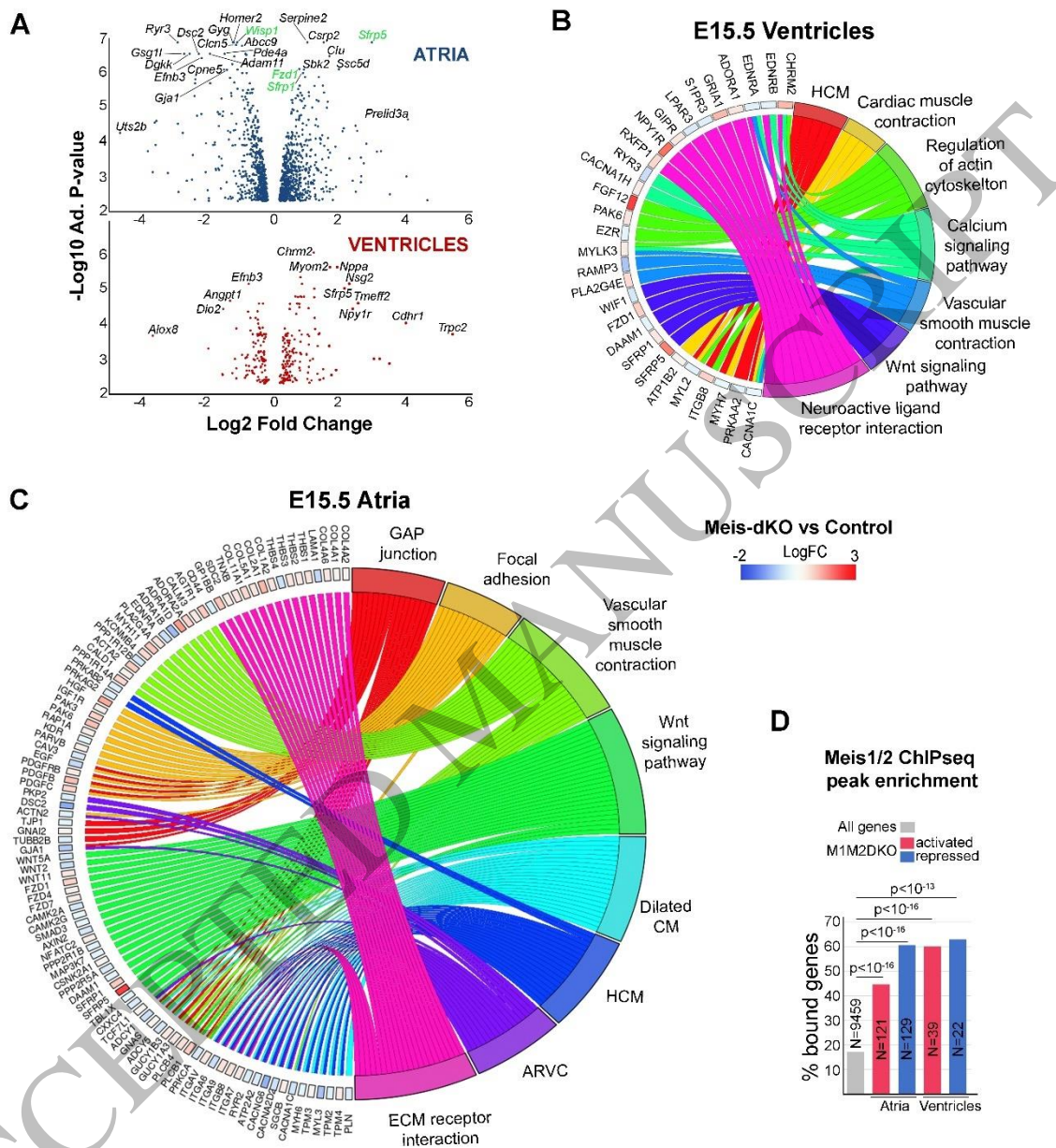


Figure 2  
200x138 mm (DPI)

1  
2  
3  
4



1  
2  
3  
4

Figure 3  
173x189 mm (DPI)

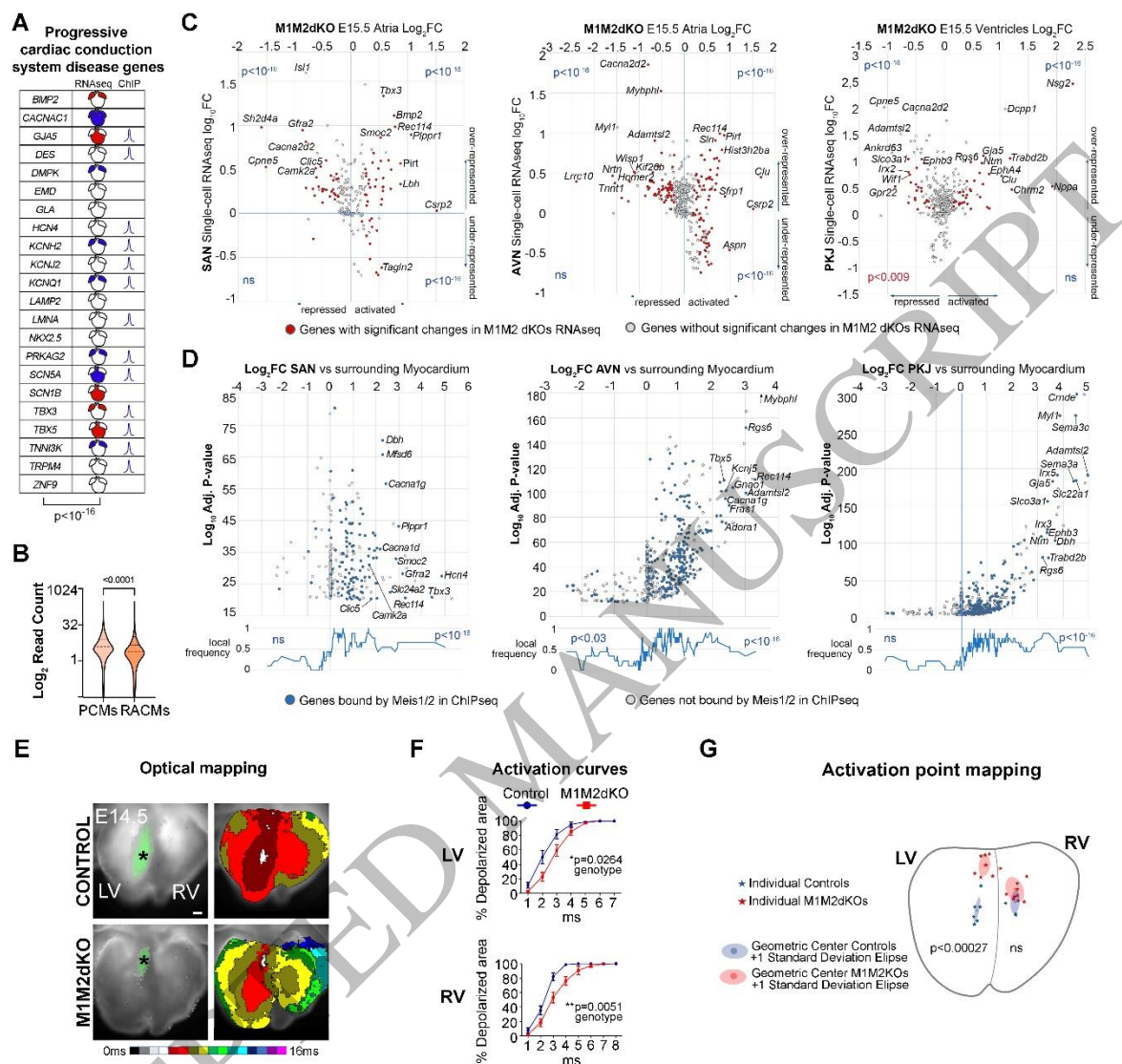
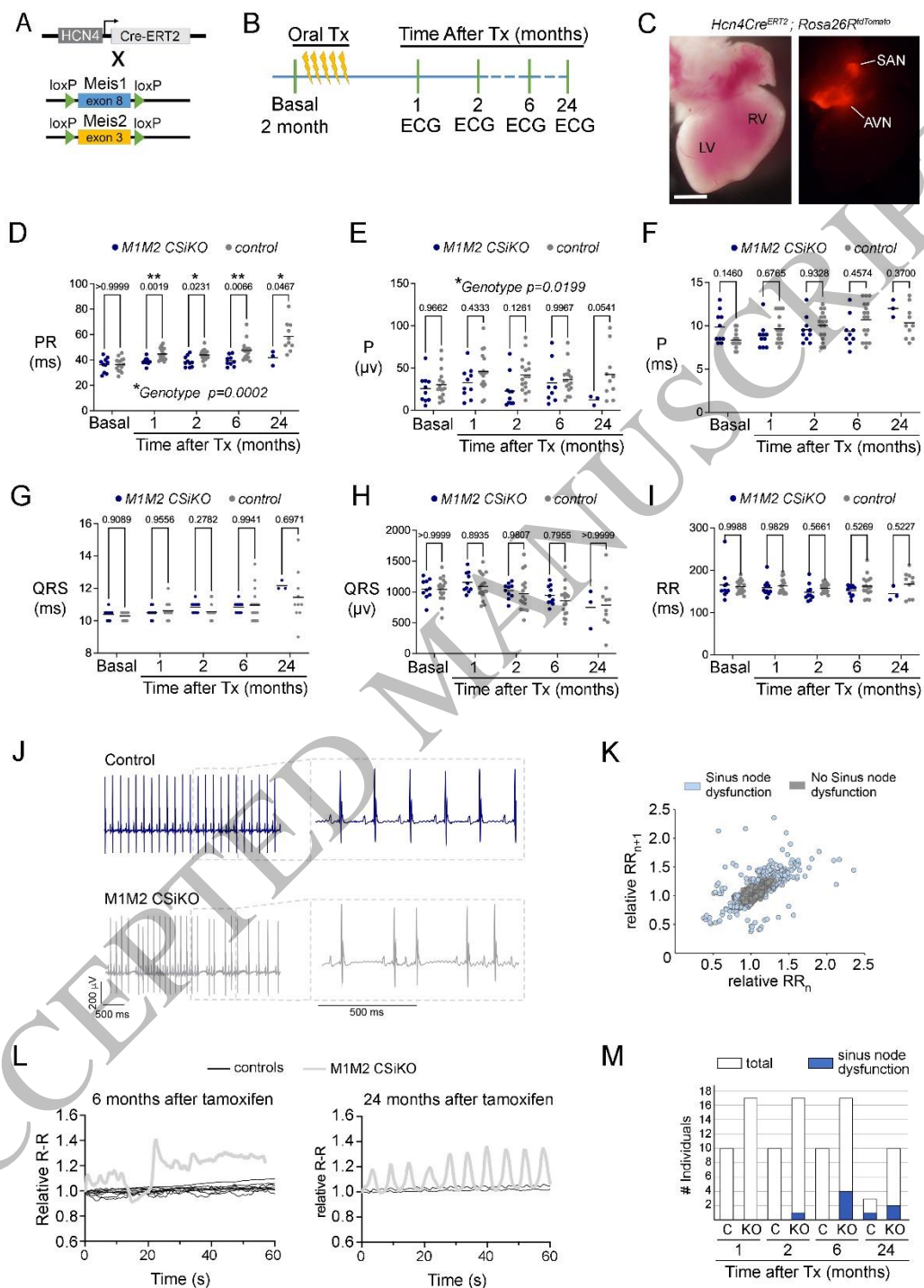


Figure 4  
207x200 mm (DPI)

1  
2  
3  
4



1  
2  
3

Figure 5  
167x220 mm (DPI)

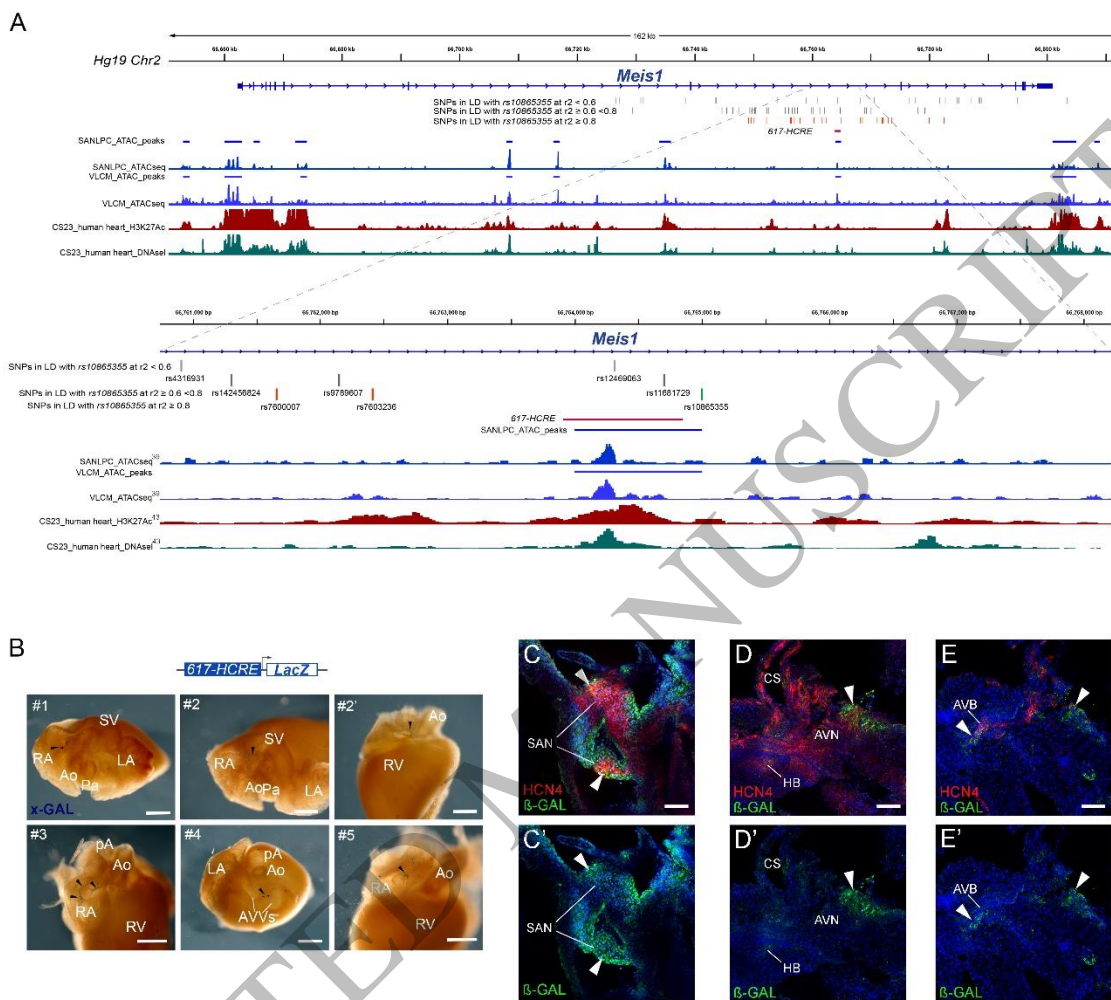


Figure 6  
210x199 mm (DPI)

1  
2  
3